Nuclear Inst. and Methods in Physics Research, A 1035 (2022) 166789

Contents lists available at ScienceDirect

Nuclear Inst. and Methods in Physics Research, A

journal homepage: www.elsevier.com/locate/nima

Experimental study of the ^{34m}Cl beam production at intermediate energies

O.A. Shehu [a,1], B.P. Crider [a,*], T. Ginter [b], C.R. Hoffman [c], T.H. Ogunbeku [a], Y. Xiao [a,b], K.L. Childers [b,d], P. Chowdhury [e], C. Fry [b,f,2], E. Lamere [e], R. Lewis [b,d], S.N. Liddick [b,d], B. Longfellow [b,f,3], S. Lyons [b,4], S.K. Neupane [g], D. Pérez-Loureiro [g,5], C.J. Prokop [h], A.L. Richard [b,3], U. Silwal [a,6], D.P. Siwakoti [a,7], D.C. Smith [a], M.K. Smith [b]

[a] Department of Physics and Astronomy, Mississippi State University, Mississippi State, MS 39762, USA
[b] National Superconducting Cyclotron Laboratory, Michigan State University, East Lansing, MI 48824, USA
[c] Physics Division, Argonne National Laboratory, Argonne, IL 60439, USA
[d] Department of Chemistry, Michigan State University, East Lansing, MI 48824, USA
[e] Department of Physics, University of Massachusetts Lowell, Lowell, MA 01854, USA
[f] Department of Physics and Astronomy, Michigan State University, East Lansing, MI 48824, USA
[g] Department of Physics and Astronomy, University of Tennessee, Knoxville, TN 37996, USA
[h] Los Alamos National Laboratory, Los Alamos New Mexico 87545, USA

ARTICLE INFO

MSC:
00-01
99-00

Keywords:
β decay
Isomeric state
γ rays

ABSTRACT

The isomeric content of a ^{34}Cl beam produced in the intermediate-energy projectile fragmentation of a 150 MeV/u ^{36}Ar beam on a 3 mm-thick Be target was studied. β-delayed γ-ray spectroscopy was used to measure the population of ^{34}Cl fragments in the ground vs. isomeric states at zero degrees relative to the incoming primary beam for four different momentum settings of the fragment separator near the predicted central velocity of these fragments, as well as, at two non-zero-degree settings for one momentum setting. Of the settings explored, which excluded rigidities within 0.5% of the value predicted to maximize total ^{34}Cl yield due to unreacted primary beam, the maximum rate for the production of ^{34m}Cl was found at a rigidity setting 0.75% below the predicted peak ^{34}Cl yield. The maximum population of the isomeric state relative to the ground state was observed at a rigidity 1.25% below the predicted maximum ^{34}Cl yield. Studies such as this are important in generating the understanding needed for producing isomer-enriched rare-isotope beams.

1. Introduction

Radioactive ion beams continue to play a central role in the forefront of nuclear science research. A sub-class of available radioactive ion beams are those whereby the isotope of interest is produced and delivered not in the lowest-lying energy (ground) state but in a metastable, so-called isomeric state (see Ref. [1] and references therein). The formulation and description of isomeric states in nuclei is a sub-field of research on its own which has produced a number of insights into our understanding of nuclei and the forces that govern them. The usefulness of isomeric beams themselves for in-beam or reaction-type experiments has also been realized, as demonstrated in Refs. [2–10]. Such measurements are able to provide new complementary information compared to the available data on isotopes residing in their ground states. Hence, there is continued motivation to develop an improved understanding of isomeric beam production mechanisms and predictions of their rates and purities at accelerator facilities worldwide.

There are numerous methods available to produce radioactive beams containing isomeric content, for example, Isotope Separation On Line (ISOL) techniques and the utilization of fission fragments, as well as in-flight, transfer, fusion evaporation, and fragmentation reactions [11]. Few of these reactions preferentially populate isomeric states of relatively low angular momenta, or spin, $J \lesssim 8$. Furthermore, most production mechanisms rely on experimental detection to determine the isomer content of each beam of interest which may not always be practical. Two exceptions to this include the use of single,

* Corresponding author.
E-mail address: bpc135@msstate.edu (B.P. Crider).
[1] Present address: Department of Physics, University of Rhode Island, Kingston, RI 02881, USA.
[2] Present address: Los Alamos National Laboratory, Los Alamos, NM 87545, USA.
[3] Present address: Lawrence Livermore National Laboratory, Livermore, CA 94550, USA.
[4] Present address: Pacific Northwest National Laboratory, Richland, WA 99352, USA.
[5] Present address: Canadian Nuclear Laboratories, Chalk River, ON K0J 1J0, Canada.
[6] Present address: Department of Physics and Astronomy, University of Wyoming, Laramie, WY 82071, USA.
[7] Present address: Holmes community college, Goodman, MS 39079, USA.

https://doi.org/10.1016/j.nima.2022.166789
Received 21 December 2021; Received in revised form 28 March 2022; Accepted 12 April 2022
Available online 6 May 2022

multi-nucleon, or charge-changing transfer reactions and fusion evaporation reactions. Transfer reactions have a palatable framework that is able to provide reliable estimates for isomeric beam production yields and rates, for example, through calculations based on the Distorted Wave Born Approximation (DWBA). Fusion evaporation reactions, similarly, have frameworks which can provide reasonable predictions of isotope production cross sections as a function of J and excitation energy. Predicting the isomeric content of a specific isotope produced via intermediate or high-energy fragmentation is far less reliable. This is particularly the case for $J \lesssim 8$ isomeric states as noted in Ref. [12].

The present work was centered around the production of ^{34}Cl via intermediate-energy fragmentation at the National Superconducting Cyclotron Laboratory (NSCL) and the population of its $J^\pi = 3^+$ isomeric state, ^{34m}Cl, having a lifetime of $T_{1/2} = 31.99(3)$ min and residing at an excitation energy of 0.146 MeV above the $J^\pi = 0^+$ ground state, ^{34g}Cl ($T_{1/2} = 1.5266(4)$ s) [13,14]. ^{34m}Cl production has a number of similarities to that reported on for ^{38}K in Ref. [12]. Both reactions utilized fragmentation of an even-A even-N beam on a Be target at intermediate energies, specifically the removal of one proton and one neutron from the beam in each case. One notable difference, is the interchange of J and the relative lifetimes of the ground and isomeric states between ^{34}Cl and ^{38}K [14,15].

An isomeric beam of ^{34m}Cl is of interest on a number of different scientific fronts. It could be used either at the full production energy ($\gtrsim$100 MeV/u) or after it has been slowed and/or re-accelerated at the ReAccelerated (ReA) beam Facility at the Facility for Rare Isotope Beam (FRIB), for example. A beam of $^{34\ m,g}$Cl at energies of ~few - 10 MeV/u is of particular interest for nuclear astrophysics and nuclear structure studies. The determination of reaction cross sections on $^{34\ m,g}$Cl will have a direct application to the usefulness of the ^{34}S/^{32}S abundance ratio in pre-solar grain classification (see Refs. [16–19] and references therein). These solar grains, produced in the dust of cooling nova, can provide new insight into the origins of nova and the creation of the heavy elements. In addition, the single-neutron adding (d, p) reaction on $^{34\ m,g}$Cl could be carried out, where the differing initial J values of ^{34g}Cl ($J = 0^+$) and ^{34m}Cl ($J = 3^+$) will result in the select population of ^{35}Cl states through the same orbital angular momentum transfer of the neutron, analogous to Refs. [6,9]. Higher-J values become accessible in the ^{34m}Cl(d, p) reaction case, and the observation of the cross sections between the overlapping states in ^{34}Cl and ^{35}Cl can provide new insight on the single-particle contributions to mirror energy differences (MEDs) in $A = 35$ nuclei [20].

2. Experiment

The production rate of ^{34}Cl along four different slices of the momentum distribution was measured. In addition, two beam-line settings were used to explore the effects of the entrance angle of the primary beam at the target on the production rates. The ^{34}Cl yields and relative beam purities for each beam setting were determined by direct ion counting in the beam-line detectors. The isomeric ^{34}Cl content of the beam was extracted using known γ-ray transitions following the β−delayed decay of the ^{34m}Cl isomeric state [13,14].

The experiment was carried out at the National Superconducting Cyclotron Laboratory (NSCL) at Michigan State University. The ^{34}Cl beam was produced at energies around ~112–119 MeV/u by impinging a primary beam of ^{36}Ar^{18+} at 149.3 MeV/u on a 3.06 mm thick Be target. The A1900 fragment separator [21] was used to sample slices of the resulting ^{34}Cl momentum distribution by use of a 0.5% momentum selection slit at the midpoint of the A1900 in conjunction with the rigidity setting of the first half of the separator. An achromatic degrader with a thickness of 150 mg/cm^2 at the midpoint of the A1900 was used to deliver the isotopes reaching it to the final A1900 focal plane dispersed not in momentum but according to differential energy loss in the degrader as a function of nuclear charge Z. The rigidity of the second half of the A1900 was set to center the ^{34}Cl within the dispersive slits at the final focal plane. The slit-spacing was set to optimize the purity of the ^{34}Cl beam with respect to other isotopes. A 340 μm thick BC400 scintillator detector, also located at the A1900 midpoint, provided a timing signal for time-of-flight (TOF) measurements made with the downstream experimental setup.

The magnetic rigidity of the first half of the A1900 just downstream from the target are given in Table 1 for the four unique momentum settings. The settings were designed to encompass the calculated $B\rho_0 = 3.3235$ Tm corresponding to the maximum of the ^{34}Cl yield from the LISE++ fragment separator simulation code [22]. The settings ranged from $\Delta B\rho_0 = -1.75\%$ to $+0.75\%$ with respect to this value. No measurements were made from approximately $-0.5\% < \Delta B\rho_0 < +0.5\%$ because the rate from the unreacted ^{36}Ar primary beam was too high for our setup at the A1900 midpoint. In addition, the two settings which introduced angles into the incoming primary beam onto the production target in the dispersive direction are also listed, where both positive and negative angles were measured for completeness. These settings (settings 5 and 6), were based on the $B\rho_{1,2}$ of setting 1 and represented the minimum and maximum angles allowed by the beam line geometry upstream from the target, ~ ±3 degrees, without observing significant loss of incoming beam intensity. The beam-on and beam-off times for each setting, t_0 and t_1, respectively, are given in Table 1. The data was continuously acquired for the full beam-on and beam-off cycles between times t_0 and t_2, while the A1900 settings were changed during the beam-off time between times t_1 and t_2. Subsequent analysis was performed for the entirety of a beam on/off cycle (t_0 to t_2). During the beam-off cycles, the currents measured for the fully-stripped ^{36}Ar primary beam were 0.014 enA, 0.0046 enA, 0.0165 enA, and 0.0235 enA for settings 1 through 4, respectively.

The secondary beam was delivered from the A1900 fragment separator to the experimental end station for each separator and beam setting (Table 1), where the composition of the beam at the experimental end station was the same as that observed at the A1900 focal plane. The experimental setup consisted of 3 silicon PIN detectors with thicknesses of 503 μm, 488 μm, and 1041 μm, a $CeBr_3$ implantation detector with dimensions 51 mm × 51 mm × 3 mm, 15 $LaBr_3$ detectors with 1.5-inch right cylindrical crystals [23], and 16 HPGe detectors which comprised the Segmented Germanium Array (SeGA) [24]. The first PIN detector was used for particle identification via its energy loss (ΔE) and the relative time-of-flight (TOF) obtained between it and the A1900 scintillator, with the others being present for redundancy. The 3-mm-thick $CeBr_3$ implantation detector was coupled with a Hamamatsu H13700 16 × 16 Position Sensitive Photo Multiplier Tube (PSPMT), as shown in Fig. 1(a). The $CeBr_3$ implantation detector signals confirmed the transmission of all ions from the PIN detectors and LISE++ calculations indicated that all ions stopped within the detector. The 16 SeGA detectors surrounded the $CeBr_3$ implantation detector for use in γ-ray detection [Fig. 1(b) and (c)]. This SeGA configuration is called the "betaSeGA" configuration. At 662 keV, the SeGA had a nominal energy resolution and efficiency of 0.86 keV and 4.48%, respectively. The $LaBr_3$ detectors were not used in the present analysis. A schematic view of the experimental setup with the detectors described above and showing the beam direction is given in Fig. 1(d).

Each detector sub-system was readout through a digital data acquisition system utilizing XIA PIXIE-16 modules [25]. Data were collected without the need of a master trigger requirement. Due to the overall low ion implantation rate (< 1 – 2 kHz), there were no lost events due to dead-time in this so-called trigger-less mode. The rates at which the incoming signals were digitized were 100 MHz for SeGA, 500 MHz for the $CeBr_3$ energy, and 250 MHz for the $CeBr_3$ positions. The timestamp information associated with the PIN detector beam ion events and the SeGA γ-ray events was used to determine the relative beam-on/data-collection start (t_0), beam-off (t_1), and data-collection stop (t_2) times (Table 1). In addition, the acquisition remained running continuously throughout the entirety of the measurements, hence, the time stamps provided accurate relative times between different settings as well,

Table 1
The percent offset from the calculated Bρ of maximum ^{34}Cl yield, $\Delta B\rho_0$, the corresponding magnetic rigidity values, $B\rho_{1,2}$, of the first two A1900 dipoles, and the ^{34}Cl energy at the A1900 Focal Plane, are listed for each of the six beam settings. The beam-on (t_0), beam-off (t_1), and data-collection stop (t_2) times are also given for each setting.

	$\Delta B\rho_0$ [%]	$B\rho_{1,2}$ [Tm]	^{34}Cl Energy [MeV/u]	t_0 [$\times 10^3$ s]	t_1	t_2
1	+0.75	3.3484	118	0.0	7.1	11.1
2	−0.75	3.2985	115	11.1	14.8	17.7
3	−1.25	3.2819	114	17.7	22.1	28.9
4	−1.75	3.2653	112	28.9	34.0	42.2
5[a]	+0.75	3.3484	118	42.2	45.8	48.3
6[b]	+0.75	3.3484	118	48.3	51.1	56.5

[a]A +3° angle was introduced into the primary beam onto the production target.
[b]A −3° angle was introduced into the primary beam onto the production target.

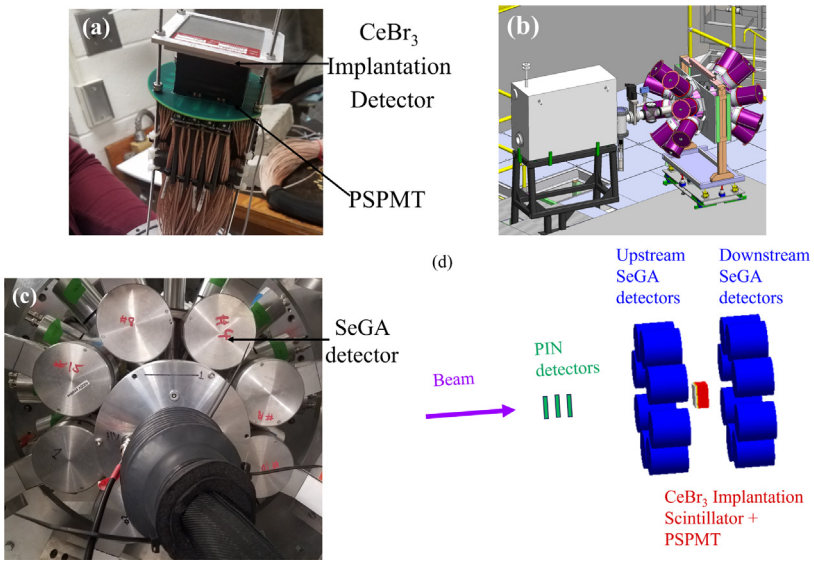

Fig. 1. (a) An image of the PSPMT coupled with the $CeBr_3$ implantation detector. (b) A drawing of the experimental end station used in the isomer determination. (c) An image of the experimental beam pipe looking upstream, showing the 8 HPGe SeGA detectors surrounding the beam pipe containing the $CeBr_3$ implantation detector. (d) Schematic view of the experimental setup and detectors used for data analysis relevant to this work.

i.e. for beam settings other than 1, the start times, t_0 equal the data collection stop times, t_2 of the previous setting.

A standard use of the "betaSeGA" configuration has been the detection of implanting ions followed by correlations with the subsequent decays. However, the relatively long lifetime of ^{34m}Cl ($T_{1/2}$ = 31.99 min) did not allow for such a correlated analysis. Instead, the rate and total number of γ-rays belonging to the ^{34m}Cl decays was accounted for over fixed time ranges (Table 1).

To determine the content of ^{34m}Cl in the beam through the number of γ rays that were emitted, a calibration of the energy, ϵ, and energy-dependent absolute efficiency of the SeGA array, was carried out. A NIST standardized source comprised of ^{154,155}Eu was used for the efficiency determination and the energy calibration. A linear energy calibration was applied and monitored throughout the measurement by comparison with known background γ rays. A GEANT4 [26] simulation was utilized to mimic the experimental setup and deduce the energy-dependent behavior of the γ-ray detection efficiency. The simulation was validated through a comparison of the data taken with the NIST source placed on the face of the $CeBr_3$ implantation detector. No impact on the efficiency (ϵ) was observed for the energy region of interest when variations in implant depths of ^{34}Cl within the $CeBr_3$ were explored across each beam setting. Fig. 2(a) shows the GEANT4 geometry for the 8 downstream SeGA detectors. Fig. 2(b) shows the resulting simulated efficiency for beam setting 1, plotted on a log–log scale for easy fitting of the parameters. A conservative systematic uncertainty of 5% was adopted over the energy region of interest (E_γ ~1 - 3.5 MeV). This is based on a comparison of the simulation with the source data at the lower energies, where efficiencies are most sensitive, and to account for the extrapolation of the efficiency function beyond the maximum source energy, E_γ ~1.4 MeV.

3. Analysis & results

Fig. 3(a) shows the ^{34}Cl rates determined at the exit focal plane of the A1900 as a function of $\Delta B\rho_0$ for the first four settings. The yields for the primary beam angle settings (settings 5 and 6 of Table 1) are not included because of the extra uncertainty associated with the ^{36}Ar primary beam current measurement. The ^{34m}Cl isomer content relative to the total ^{34}Cl beam, as determined at the detector station, is shown in Fig. 3(b) for all four $\Delta B\rho_0$ settings, as well as the two primary-beam angle settings. The black bands in the horizontal direction on each data point illustrate the 0.5% momentum acceptance sampled in each beam setting (Table 1). The gray shaded bands in Figs. 3(a) and (b) define the excluded region due to the acceptance of the primary beam ^{36}Ar on the A1900 timing detector. The orange histogram in Fig. 3(a) shows the prediction for the ^{34}Cl yield as a function of $\Delta B\rho_0$, with the peak of the distribution being placed at 0, from the LISE++ fragment separator simulation code (version 12.1.2 with option and configuration file "A1900_2019") [22]. The $^{36}Ar^{18+}$ primary beam current was relatively low (< 0.1 enA) as required to keep the implant rates reasonable. This resulted in some intensity fluctuations and a systematic uncertainty of ~10% on the extraction of the A1900 rates in pps/pnA.

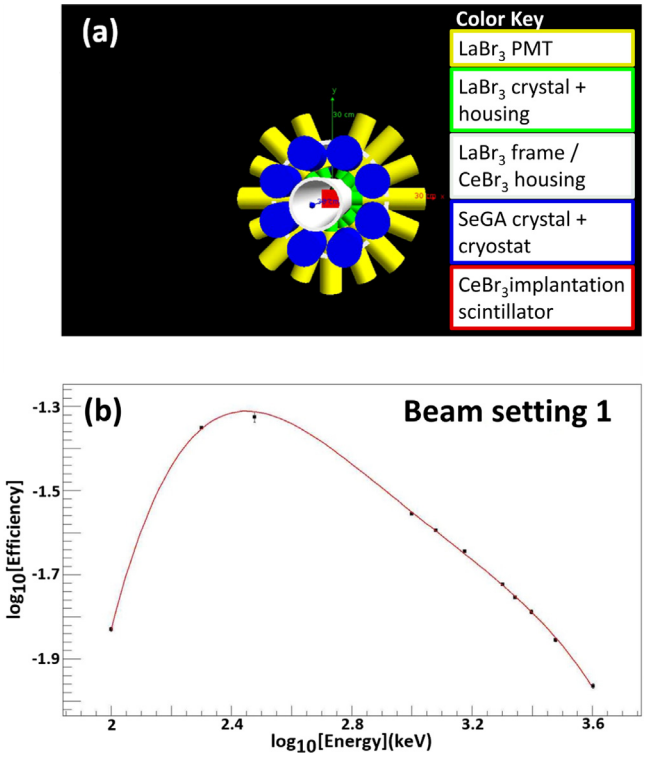

Fig. 2. (a) The geometry of the experimental setup as viewed in the GEANT4 simulation used for the energy-dependent efficiency determination of the SeGA. (b) The resulting energy-dependent efficiency curve ϵ for setting 1 (solid line). The data points indicated in black are the γ-ray energies used for the simulated data after validating the configuration with a standardized source.

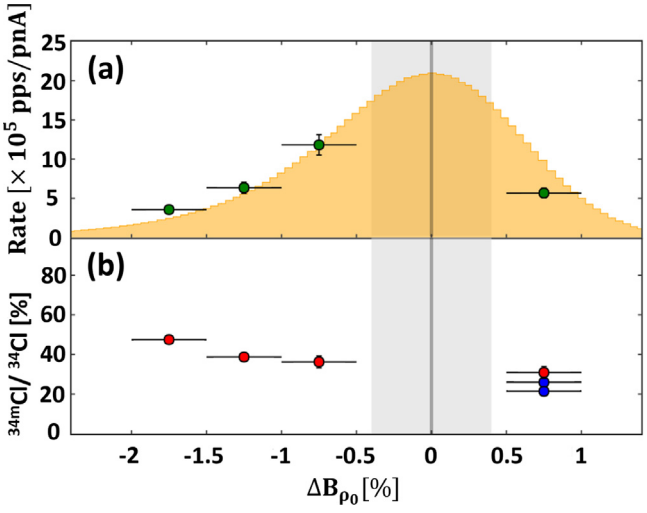

Fig. 3. (a) The measured ^{34}Cl beam rates at the A1900 separator Focal Plane (FP) (green points with error bars) normalized to incoming beam current as measured at the target position are given as a function of the percent in rigidity off from the LISE++ expected maximum rate ($\Delta B\rho_0$). The distribution of the estimated rates from LISE++ are also shown for ^{34}Cl (orange filled histogram) and they have been scaled to the measured ^{34}Cl beam-rate data. (b) The measured isomer fraction in the ^{34}Cl beam at the experimental end station, ^{34m}Cl/^{34}Cl, is shown for the four $\Delta B\rho_0$ settings (red points) as well as the two primary beam angle settings (blue points). In both (a) and (b) the horizontal bars on each data point indicate the 0.5% momentum acceptance of the A1900 separator and the vertical error bars are shown when greater than the size of the data point. The gray band in both (a) and (b) also identifies the excluded momentum region of the measurement due to overlap with the unreacted ^{36}Ar primary beam Bρ.

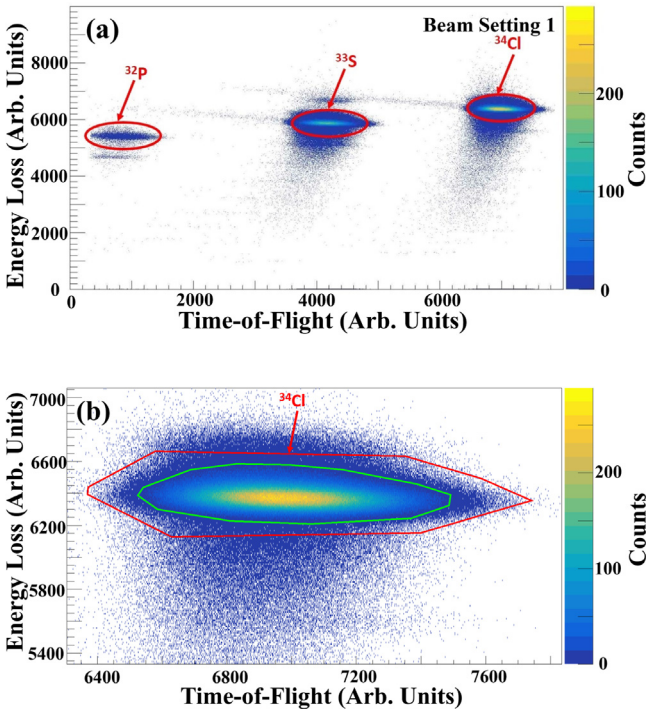

Fig. 4. (a) A representative particle identification plot for beam setting 1, consisting of the energy loss ΔE in the first PIN detector and the TOF between the A1900 scintillator and the first PIN detector. (b) Examples of varying sizes of graphical cuts explored to determine the total number of ^{34}Cl beams ions for beam setting 1.

Fig. 4 shows a typical particle-identification (PID) plot for beam setting 1. The isotope of interest,^{34}Cl, was identified based on comparisons with reference PID plots made at the A1900 fragment separator Focal Plane, which are also based on measurements of energy loss vs. time-of-flight, and easily separated from other beam contaminants. In addition to the beam contaminants,^{32}P and ^{33}S, shown in Fig. 4,^{35}Ar was also observed in settings 3 and 4.^{33}S, being a stable nucleus, was not observed in the gamma ray spectra, as well as decays from ^{32}P because of its long half life of 14.268(5) days [27] compared to the implantation rate. ^{35}Ar with $T_{1/2} \approx 1.78$ sec, allowed for a correlated implant plus decay via a 1.23% decay branch and the 1219.3(2) keV γ ray [28] during beam setting 4. Thus, the ^{34}Cl selection in the PID was independently corroborated from A1900 fragment separator PID reference plots. Finally, the transmission of ^{34}Cl beam ions from the first PIN detector to the $CeBr_3$ implantation detector, a distance of ~1 m, was determined to be ~100%. This was deduced through the ratio of counts in the $CeBr_3$ PSPMT dynode energy with the corresponding number of counts observed in first PIN ΔE signal over a fixed time period.

The average implant rate of the$^{34\ g,m}$Cl beam was calculated by taking the integral of a graphical cut made on the ^{34}Cl region encompassing the beam-on time period for each setting ($t_0 \rightarrow t_1$). Uncertainties due to the size and shape of the graphical cut were explored for each setting, see for example, the two different graphical cuts in Fig. 4(b). Similar to the A1900 rate determinations, an additional systematic uncertainty of ~10% was included due to possible fluctuations in the primary beam current.

In order to interpret the present data, a review of the known β-delayed γ-ray decay scheme of ^{34}Cl was necessary [13,14] (Fig. 5). The ^{34}Cl isotope has two known long-lived beta-decaying states namely, the ground state (^{34g}Cl, $J^\pi = 0^+$) and the isomeric state (^{34m}Cl, $J^\pi = 3^+$) state. The decay of^{34g}Cl has a half life of 1.5266(4) s and decays via β^+ into the ground state of ^{34}S with a branching ratio of 100%, producing no γ-ray transitions.^{34m}Cl has a half life of 31.99(3) minutes and can decay via β^+ decay with a branching ratio of 54.3% (with

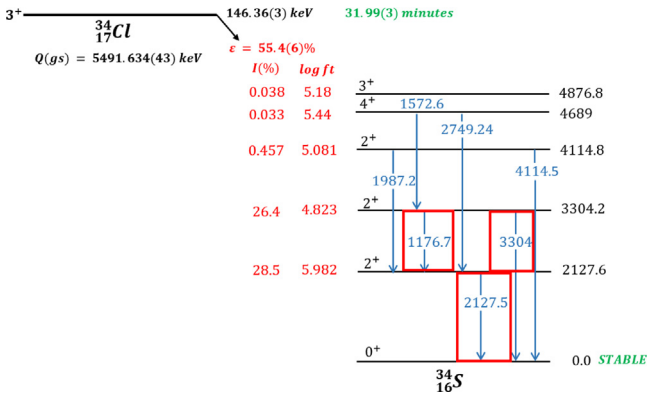

Fig. 5. The previously deduced β^+ decay scheme of ^{34m}Cl ($J^\pi = 3^+$, $T_{1/2}$ = 31.99(3) minutes) with a branching ratio of 55.4(6)% [13,14]. The red boxes indicates the three γ rays utilized in the present work.

a 1.1% electron capture branch, summing to a decay branch total of 55.4%) or internal transition with a branching ratio of 44.6%, where this latter branch is split between emission of a 146-keV γ ray (38.3%) and conversion electron emission (6.3%). The 146-keV transition was largely suppressed by the $CeBr_3$ implantation detector and the little yield that was observed by the SeGA detectors sat upon the Compton background and thus carried large statistical uncertainties. Therefore, it was not used in the final analysis. The β^+ decay of ^{34m}Cl results in 3 easily observable higher-energy γ-ray transitions, the 1176.650(20) keV $2_2^+ \rightarrow 2_1^+$, the 2127.499(20) keV $= 2_1^+ \rightarrow 0_1^+$, and the 3304.031(20) keV $= 2_2^+ \rightarrow 0_1^+$.

The complete set of the six different beam settings may be visualized from the plot of the γ-ray energies versus their corresponding time stamp values in Fig. 6. The six vertically dense areas on Fig. 6 show the beam-on periods. The red lines in the figure identify the 1177-, 2127-, and 3304-keV γ-transitions following the decay of ^{34m}Cl. To determine the rate of ^{34m}Cl for each beam setting, a projection on to the SeGA energy axis of Fig. 6 was taken encompassing $t_0 < t < t_2$ (Table 1). Fig. 7 shows typical γ-ray energy spectra, without energy-dependent efficiency corrections, for the transitions of interest over the first beam-setting time range. Each γ-ray peak was fitted using a Gaussian function and a linear background to extract the number of counts. The same fitting method was applied to all six settings. The resulting numbers of raw counts of the ^{34m}Cl γ-rays of interest are shown in Table 2 along with their associated uncertainties.

The decay branching ratios BR (Fig. 5) and SeGA efficiency corrections, ϵ, were implemented on number of counts extracted for each ^{34m}Cl γ ray, A_m, to determine the number of ^{34m}Cl decays, N_d, which took place over each $t_0 \rightarrow t_2$ measuring period. Namely,

$$N_d = \frac{A_m}{\epsilon(\mathrm{E}_\gamma) \times BR}. \quad (1)$$

The energy-dependent efficiencies of SeGA were determined to be ϵ(1177 keV) = 3.2(2)%, ϵ(2127 keV) = 2.3(1)% and ϵ(3304 keV) = 1.6(1)%. As noted in Section 2, the dependence of the efficiency was explored independently for each beam setting and no significant variations were observed. The branching ratios of the 3 γ-rays of interest were taken from Refs. [13,14], i.e., BR = 14.09(24)%, 42.8(8)% and 12.29(22)%, in increasing γ-ray energy, respectively. The resulting N_d are given in Table 2. Uncertainties include those from the efficiency and branching ratios, as well as those from statistics. The N_d for the 3304-keV transitions was found to be reduced systematically across all settings, however, it was within the quoted uncertainties.

The rate of the isomeric ^{34m}Cl beam component, R_m, was extracted from the deduced N_d of each γ ray (Table 2) after correcting for any previous beam-on decay events, C_d, and then normalizing to the expected number of decay events which accounted for the half-life of the isomeric state during the build-up/beam on ($t_0 \rightarrow t_1$) and decay ($t_1 \rightarrow t_2$) portions of the measuring period, E_d. Standard exponential equations were used to estimate the build-up and decay terms. The full expression is represented as,

$$\begin{aligned} N_d - C_d &= R_m \cdot E_d \\ E_d &= \int_{t_0}^{t_1} (1 - e^{-\lambda(t-t_0)})dt + \int_{t_1}^{t_2} e^{-\lambda(t-t_1)}dt \\ C_d &= \overline{R_m}' [\int_{t_0}^{t_2} e^{-\lambda(t-t_1')}dt]. \end{aligned} \quad (2)$$

t_0 is the time the beam was turned on, t_1 the time when the beam was stopped, and t_2 the time when data collection ended, all in seconds (see Table 1). $\lambda = ln(2)/T_{1/2} = 0.000361$ [1/sec] based on the known isomer lifetime of 31.99 min [14]. Each *primed* variable indicates values taken from previous beam settings. The weighted average of the individual R_m for the six settings, $\overline{R_m}$, are given in Table 3. The other values of Eq. (2) are listed in Table 2. While the long half-life of ^{34m}Cl meant that saturation did not necessarily occur for each beam setting, the $\sim$ 100% transmission and implantation of beam ions, coupled with the use of known γ-ray intensities for our analysis, meant that we could still accurately count the decays and implanted ions such that the only impact for not achieving saturation was improved counting statistics.

A constant incoming beam rate was assumed over the beam on period, however as noted above, fluctuations were observed in the direct measure of the overall rate. Therefore, a systematic uncertainty of $\sim$10% has also been added to the ^{34m}Cl rate determinations. Because extraction of the isomer fractions relied only on the ratios of the ^{34m}Cl and ^{34}Cl rates, fluctuations in the primary beam current did not play a leading role in their associated uncertainties. For the C_d correction term of Eq. (2), $\overline{R_m}'$ was $\equiv 0$ for setting 1. In most cases this correction was $\leq$ 6% except for settings 3 and 6, which were impacted at the $\sim$20% level due to their close proximity to the previous beam-on periods (Table 2).

4. Discussion

Based on the results presented in Table 3 and Fig. 3, the maximum rate of the ^{34m}Cl isomeric beam over the $\Delta B\rho_0$ region probed was found for the $\Delta B\rho_0 = -0.75\%$ setting. However, this setting has a reduced ratio of isomer to ground state, ^{34m}Cl/^{34}Cl $\approx$36%, relative to other settings. In particular, the largest ^{34m}Cl fraction could be found at the largest momentum setting explored, $\Delta B\rho_0 = -1.75\%$, though at a reduced overall production rate.

A comparison is made with the ^{38m}K isomer production study of Ref. [12] in terms of the trends of the isomer-to-ground state content as a function of $\Delta B\rho_0$. As noted in the introduction, these two nuclei have similar structure, only with an inversion of the energy-ordering of the $J^\pi = 0^+$ and 3^+ states. Also, the production method of Ref. [12] is analogous to present work. Both of these relatively low-J isomers are populated with fractions ranging from $\approx 30-60\%$ via intermediate energy fragmentation. For reference, via fragmentation of ^{58}Ni, the estimated isomer population of the much higher $J = 19/2^-$ isomeric state in ^{53}Co was $\approx$ 27% [5]. Both studies also find that a modification of the primary beam angle on the production target had no positive effect on increasing the isomer fraction (blue points in Fig. 3).

The maximum value of the isomer content is similar for both ^{34m}Cl and ^{38m}K for the $\Delta B\rho_0$ regions that were investigated ($\sim 50-60\%$). The maximum ^{34m}Cl fraction observed lies at $\Delta B\rho_0 = -1.75\%$, while the ^{38m}K fraction observed peaked at $\Delta B\rho_0 = +1\%$. Also, the ^{34m}Cl component was found to increase with larger separation from $B\rho_0$, opposite to the trend of the ^{38m}K component. The differing trends in production of ^{34m}Cl and ^{38m}K are possibly related to the interchange of the isomer and the ground state J^π values. Namely, it appears that the relative yields to the 3^+ levels increase over the 0^+ levels resulting in increased isomer production in ^{34}Cl and increased ground state production in ^{38}K. Even though the states involved are relatively low-spin, it is possible the

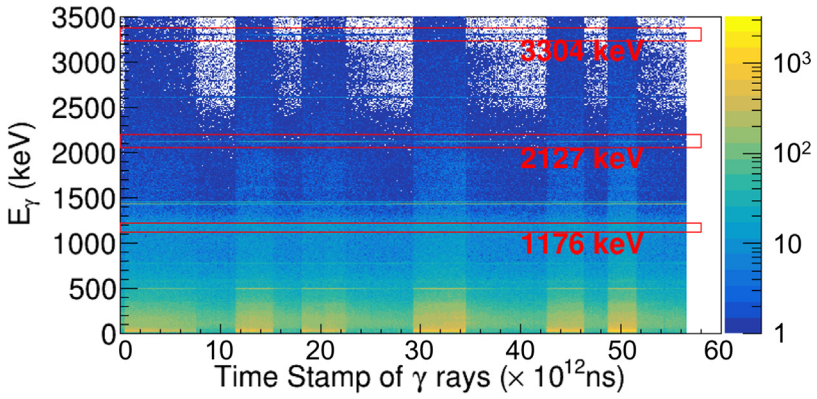

Fig. 6. The energy versus timestamp data in nanoseconds for the γ rays detected by SeGA. The six vertically dense bands show the beam-on periods of each setting. Additionally, the 1177-, 2127-, and 3304-keV, transitions corresponding to the decay of ^{34m}Cl are indicated on the plot by the red bands.

Table 2
The extracted number of counts and the deduced number of ^{34m}Cl decays (N_d) are listed for each γ ray of interest along with their associated uncertainties. For each setting, the number of decay events corresponding to the previous beam-on period (C_d), and the expected number of decay events per isomer implant rate (E_d), described in Eq. (2), are listed with their associated uncertainties.

	E_γ [keV]	Counts [×10^3]	N_d [×10^5]	C_d [×10^5]	E_d[a] [×10^3]
1	1177	2.40(17)	5.28(47)	–	6.66
	2127	5.14(12)	5.26(31)		
	3304	0.908(63)	4.82(42)		
2	1177	3.77(16)	8.31(56)	0.46(5)	3.46
	2127	8.02(15)	8.24(46)		
	3304	1.420(64)	7.51(52)		
3	1177	4.72(19)	10.32(68)	2.09(21)	4.73
	2127	9.73(16)	9.95(55)		
	3304	1.680(69)	8.92(60)		
4	1177	6.45(22)	14.22(89)	0.40(4)	5.40
	2127	14.46(20)	14.70(81)		
	3304	2.651(89)	14.00(88)		
5	1177	2.38(15)	5.27(43)	0.33(3)	3.23
	2127	4.99(12)	5.13(30)		
	3304	0.873(58)	4.68(40)		
6	1177	3.87(18)	8.60(60)	1.55(16)	3.41
	2127	8.30(17)	8.49(48)		
	3304	1.546(74)	8.15(59)		

[a]All values have been assigned a systematic uncertainty of ~10%.

Table 3
The ^{34}Cl beam rates measured at the A1900 Focal Plane (FP) are listed for the first four settings, settings 5 and 6 did not allow for accurate primary beam current measurements. The ^{34}Cl beam purity and implant rates are also given along side the extracted ^{34m}Cl isomer implant rates ($\overline{R}_m$) and the ^{34m}Cl percent ($/^{34}$Cl) in the composite ^{34}Cl beam. An approximate measure of total ^{34m}Cl rate for each setting based on the A1900 FP rates, is shown the last column. For this case, the rates have been normalized to the maximum value which was found for setting 2. Systematic and statistical uncertainties have been included (see text for additional details.).

Setting	$\Delta B\rho_0$	^{34}Cl			^{34m}Cl		
	[%]	A1900 FP rate [×10^5 pps/pnA]	Implant rate [pps]	Purity [%]	$\overline{R}_m$ [pps]	$/^{34}$Cl [%]	$/^{34}$Cl× A1900 FP rate [arb. units]
1	+0.75	5.7(6)	250(27)	56.4	77(9)	31(2)	~40
2	−0.75	11.8(12)	604(66)	84.1	219(23)	36(2)	~100
3	−1.25	6.4(7)	415(45)	86.1	162(17)	39(3)	~60
4	−1.75	3.6(4)	544(60)	54.5	258(27)	47(3)	~40
5	+0.75	–	561(61)	52.8	145(17)	26(2)	–
6	+0.75	–	939(102)	58.5	201(22)	21(2)	–

$\Delta J = 3$ is large enough to contribute to variations in the population irrespective of excitation energy. As noted in Ref [29], the width of the residue momentum distributions in the direct removal of a neutron-proton pair can vary significantly depending on the final state. For ^{34}Cl and ^{38}K, the $J = 0^+$ and $J = 3^+$ states arise from the same underlying single-particle structure. The similar production mechanisms used for ^{34m}Cl in this work and ^{38m}K in the work of Ref. [12], i.e., the likely removal of a $1d_{3/2}$ neutron and a $1d_{3/2}$ proton from the primary beam in both cases, suggests the population of the 0^+ and 3^+ states in both ^{34}Cl and ^{38}K could be expected to be similar with the momentum widths being largely governed by the angular momentum component of the LS decomposition of the two nucleon overlap. Therefore, comparatively wide $J = 3^+$ and narrow $J = 0^+$ momentum distributions qualitatively explain the observation of an increased yield to the $J = 3^+$ level relative to the $J = 0^+$ level further from the central momentum or calculated $B\rho_0$ in ^{34}Cl, as well as what is reported in Fig. 3 of Ref. [12]. Detailed

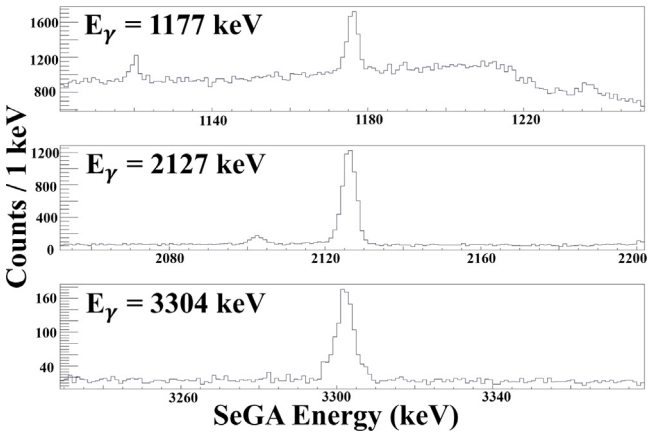

Fig. 7. Projected γ-ray spectra from Fig. 6 onto the energy axis for the ^{34m}Cl lines of interest encompassing the time duration $t_0 \rightarrow t_2$ of setting 1 (Table 1).

calculations for these nuclei are complicated due to the competition between direct and indirect contributions to the reaction yields, and hence, are beyond the scope of the present work. The concept is further emphasized considering that the majority of bound excited states with larger J values ($J \gtrsim 3$) are known to preferentially feed into the 3^+ over the 0^+ in these isotopes [14,15].

It is worth noting, as explored in Ref. [12], that some control over the fraction of the isomer content may also be found through variation of the length of the charge breeding time. For example this would take place in an Electron Beam Ion Trap/Source (EBIT/S) at the ReA Facility at FRIB. In terms of ^{34}Cl, stretching the charge-breeding time would increase the fraction of the longer-lived isomer ($T_{1/2} \approx 32$ mins) relative to the shorter-lived ground state ($T_{1/2} \approx 1.6$ sec). For the ratio of ^{34m}Cl/^{34}Cl, a charge breeding time of 2000 ms (the maximum charge breeding time reported in Ref. [12]) could result in an improvement up to roughly a factor of 2. Of course, the total amount of ^{34}Cl would also diminish under these conditions.

5. Summary

In summary, we have measured the beam production rates and isomeric state composition of ^{34m}Cl via fragmentation at the NSCL using different momentum settings of the A1900 fragment separator to sample unique slices of the ^{34}Cl momentum distribution. The $\Delta B\rho = -0.75\%$ setting of the A1900 yielded the maximum rate of the ^{34m}Cl isomeric beam, while the largest ^{34m}Cl fraction is found at $\Delta B\rho_0 = -1.75\%$. Comparison to a similar study on ^{38m}K production [12] yields the interesting result that the isomeric state rates are maximized on opposite sides of their respective momentum distributions. This difference could possibly be attributed to the spin difference between the $J^\pi = 0^+$ states (^{34g}Cl and ^{38m}K) and the $J^\pi = 3^+$ states (^{34m}Cl and ^{38g}K). The new information on isomeric state beam production will help provide guidance towards future experiments reliant on such beams.

CRediT authorship contribution statement

O.A. Shehu: Software, Formal analysis, Writing – original draft, Writing – review & editing, Visualization. **B.P. Crider:** Conceptualization, Software, Formal analysis, Writing – original draft, Writing – Review & Editing, Visualization, Supervision, Resources, Project administration. **T. Ginter:** Conceptualization, Investigation, Formal analysis, Writing – original draft, Writing – review & editing, Visualization. **C.R. Hoffman:** Conceptualization, Investigation, Formal analysis, Writing – original draft, Writing – review & editing, Visualization, Project administration. **T.H. Ogunbeku:** Investigation, Software, Writing – review & editing, Visualization. **Y. Xiao:** Investigation, Software, Visualization. **K.L. Childers:** Investigation. **P. Chowdhury:** Investigation, Resources. **C. Fry:** Investigation. **E. Lamere:** Investigation. **R. Lewis:** Investigation. **S.N. Liddick:** Conceptualization, Investigation, Resources, Project Administration, Supervision. **B. Longfellow:** Investigation, Writing – review & editing. **S. Lyons:** Investigation. **S.K. Neupane:** Investigation. **D. Pérez-Loureiro:** Investigation. **C.J. Prokop:** Investigation. **A.L. Richard:** Investigation. **U. Silwal:** Investigation. **D.P. Siwakoti:** Investigation. **D.C. Smith:** Investigation. **M.K. Smith:** Investigation.

Declaration of competing interest

The authors declare that they have no known competing financial interests or personal relationships that could have appeared to influence the work reported in this paper.

Acknowledgments

The authors would like to thank J. A. Winger for help in the preparation of this manuscript. This work was supported by the National Science Foundation, USA under Grant No. PHY 1848177 (CAREER) and Grant No. PHY 1565546 (NSCL). This work was supported by the U.S. Department of Energy, Office of Science, Office of Nuclear Physics, under Contract No. DE-AC02-06CH11357 (ANL). This work was supported by the US Department of Energy, Office of Science, Office of Nuclear Physics under Grant No. DE-FG02-94ER40848 (UML).

References

[1] G.D. Dracoulis, P.M. Walker, F.G. Kondev, Review of metastable states in heavy nuclei, Rep. Prog. Phys. 79 (7) (2016) 076301, http://dx.doi.org/10.1088/0034-4885/79/7/076301.

[2] T. Morikawa, Y. Gono, K. Morita, T. Kishida, T. Murakami, E. Ideguchi, H. Kumagai, G. Liu, A. Ferragut, A. Yoshida, Y. Zhang, M. Oshima, M. Sugawara, H. Kusakari, M. Ogawa, M. Nakajima, H. Tsuchida, S. Mitarai, A. Odahara, M. Kidera, M. Shibata, J. Kim, S. Chae, Y. Hatsukawa, M. Ishihara, Coulomb excitation of 174Hf K-isomer. ˆi^3-ray spectroscopy with high-spin isomer beam, Phys. Lett. B 350 (2) (1995) 169–172, http://dx.doi.org/10.1016/0370-2693(95)00345-L.

[3] H. Watanabe, K. Asahi, T. Kishida, H. Ueno, W. Sato, A. Yoshimi, Y. Kobayashi, D. Kameda, H. Miyoshi, T. Fukuchi, Y. Wakabayashi, T. Sasaki, M. Kibe, N. Hokoiwa, A. Odahara, B. Cederwall, K. Lagergren, Z. Podolyak, M. Ishihara, Y. Gono, Application of the high-spin isomer beams to the secondary fusion reaction and the measurement of g-factor, Nuclear Phys. A 746 (2004) 540–543, http://dx.doi.org/10.1016/j.nuclphysa.2004.09.141, Proceedings of the Sixth International Conference on Radioactive Nuclear Beams (RNB6).

[4] I. Stefanescu, G. Georgiev, F. Ames, J. Äystö, D.L. Balabanski, G. Bollen, P.A. Butler, J. Cederkäll, N. Champault, T. Davinson, A.D. Maesschalck, P. Delahaye, J. Eberth, D. Fedorov, V.N. Fedosseev, L.M. Fraile, S. Franchoo, K. Gladnishki, D. Habs, K. Heyde, M. Huyse, O. Ivanov, J. Iwanicki, J. Jolie, B. Jonson, T. Kröll, R. Krücken, O. Kester, U. Köster, A. Lagoyannis, L. Liljeby, G.L. Bianco, B.A. Marsh, O. Niedermaier, T. Nilsson, M. Oinonen, G. Pascovici, P. Reiter, A. Saltarelli, H. Scheit, D. Schwalm, T. Sieber, N. Smirnova, J.V.D. Walle, P.V. Duppen, S. Zemlyanoi, N. Warr, D. Weisshaar, F. Wenander, Coulomb excitation of ^{68,70}Cu: First use of postaccelerated isomeric beams, Phys. Rev. Lett. 98 (2007) 122701, http://dx.doi.org/10.1103/PhysRevLett.98.122701.

[5] S.A. Milne, M.A. Bentley, E.C. Simpson, T. Baugher, D. Bazin, J.S. Berryman, A.M. Bruce, P.J. Davies, C.A. Diget, A. Gade, T.W. Henry, H. Iwasaki, A. Lemasson, S.M. Lenzi, S. McDaniel, D.R. Napoli, A.J. Nichols, A. Ratkiewicz, L. Scruton, S.R. Stroberg, J.A. Tostevin, D. Weisshaar, K. Wimmer, R. Winkler, Isospin symmetry at high spin studied via nucleon knockout from isomeric states, Phys. Rev. Lett. 117 (2016) 082502, http://dx.doi.org/10.1103/PhysRevLett.117.082502.

[6] S. Almaraz-Calderon, K.E. Rehm, N. Gerken, M.L. Avila, B.P. Kay, R. Talwar, A.D. Ayangeakaa, S. Bottoni, A.A. Chen, C.M. Deibel, C. Dickerson, K. Hanselman, C.R. Hoffman, C.L. Jiang, S.A. Kuvin, O. Nusair, R.C. Pardo, D. Santiago-Gonzalez, J. Sethi, C. Ugalde, Study of the ^{26}Al$^m(d,p)^{27}$Al reaction and the influence of the ^{26}Al0$^+$ isomer on the destruction of ^{26}Al in the galaxy, Phys. Rev. Lett. 119 (2017) 072701, http://dx.doi.org/10.1103/PhysRevLett.119.072701.

[7] D. Kahl, H. Shimizu, H. Yamaguchi, K. Abe, O. Beliuskina, S.M. Cha, K.Y. Chae, A.A. Chen, Z. Ge, S. Hayakawa, N. Imai, N. Iwasa, A. Kim, D.H. Kim, M.J. Kim, S. Kubono, M.S. Kwag, J. Liang, J.Y. Moon, S. Nishimura, S. Oka, S.Y. Park, A. Psaltis, T. Teranishi, Y. Ueno, L. Yang, Isomer beam elastic scattering: 26mAl(p, p) for astrophysics, 165, 2017, p. 01030, http://dx.doi.org/10.1051/epjconf/201716501030.

[8] B. Asher, S. Almaraz-Calderon, O. Nusair, K. Rehm, M. Avila, A. Chen, C. Dickerson, C. Jiang, B. Kay, R. Pardo, D. Santiago-Gonzalez, R. Talwar, Development of an Isomeric beam of26Al for nuclear reaction studies, Nucl. Instrum. Methods A 899 (2018) 6–9, http://dx.doi.org/10.1016/j.nima.2018.05.015.

[9] D. Santiago-Gonzalez, K. Auranen, M.L. Avila, A.D. Ayangeakaa, B.B. Back, S. Bottoni, M.P. Carpenter, J. Chen, C.M. Deibel, A.A. Hood, C.R. Hoffman, R.V.F. Janssens, C.L. Jiang, B.P. Kay, S.A. Kuvin, A. Lauer, J.P. Schiffer, J. Sethi, R. Talwar, I. Wiedenhöver, J. Winkelbauer, S. Zhu, Probing the single-particle character of rotational states in ^{19}F using a short-lived isomeric beam, Phys. Rev. Lett. 120 (2018) 122503, http://dx.doi.org/10.1103/PhysRevLett.120.122503.

[10] B. Longfellow, D. Weisshaar, A. Gade, B.A. Brown, D. Bazin, K.W. Brown, B. Elman, J. Pereira, D. Rhodes, M. Spieker, Shape changes in the $N = 28$ island of inversion: Collective structures built on configuration-coexisting states in ^{43}S, Phys. Rev. Lett. 125 (2020) 232501, http://dx.doi.org/10.1103/PhysRevLett.125.232501.

[11] Y. Blumenfeld, T. Nilsson, P. Van Duppen, Facilities and methods for radioactive ion beam production, Phys. Scr. 2013 (T152) (2013) 014023, http://dx.doi.org/10.1088/0031-8949/2013/t152/014023.

[12] K.A. Chipps, R.L. Kozub, C. Sumithrarachchi, T. Ginter, T. Baumann, K. Lund, A. Lapierre, A. Villari, F. Montes, S. Jin, K. Schmidt, S. Ayoub, S.D. Pain, D. Blankstein, ^{38}K Isomer production via fast fragmentation, Phys. Rev. Accel. Beams 21 (2018) 121301, http://dx.doi.org/10.1103/PhysRevAccelBeams.21.121301.

[13] M. Van Driel, H. Klijnman, G. Engelbertink, H. Eggenhuisen, J. Hermans, Allowed electron-capture branches in the decay of 34mCl, Nuclear Phys. A 240 (1) (1975) 98–108, http://dx.doi.org/10.1016/0375-9474(75)90439-X.

[14] N. Nica, B. Singh, Nuclear data sheets for A=34, Nucl. Data Sheets 113 (6) (2012) 1563–1733, http://dx.doi.org/10.1016/j.nds.2012.06.001.

[15] J. Chen, Nuclear data sheets for A=38, Nucl. Data Sheets 152 (2018) 1–330, http://dx.doi.org/10.1016/j.nds.2018.10.001.

[16] J. Jose, M. Hernanz, S. Amari, K. Lodders, E. Zinner, The imprint of nova nucleosynthesis in presolar grains, Astrophys. J. 612 (1) (2004) 414–428, http://dx.doi.org/10.1086/422569.

[17] C. Iliadis, A. Champagne, J. Jose, S. Starrfield, P. Tupper, The effects of thermonuclear reaction-rate variations on nova nucleosynthesis: A sensitivity study, Astrophys. J. Suppl. Ser. 142 (1) (2002) 105–137, http://dx.doi.org/10.1086/341400.

[18] A. Coc, M.-G. Porquet, F. Nowacki, Lifetimes of ^{26}Al and ^{34}Cl in an astrophysical plasma, Phys. Rev. C 61 (1999) 015801, http://dx.doi.org/10.1103/PhysRevC.61.015801.

[19] W.A. Richter, B.A. Brown, R. Longland, C. Wrede, P. Denissenkov, C. Fry, F. Herwig, D. Kurtulgil, M. Pignatari, R. Reifarth, Shell-model studies of the astrophysical rp-process reactions ^{34}S$(p,\gamma)^{35}$Cl and ^{34g,m}Cl$(p,\gamma)^{35}$Ar, Phys. Rev. C 102 (2020) 025801, http://dx.doi.org/10.1103/PhysRevC.102.025801.

[20] J. Ekman, D. Rudolph, C. Fahlander, A.P. Zuker, M.A. Bentley, S.M. Lenzi, C. Andreoiu, M. Axiotis, G. de Angelis, E. Farnea, A. Gadea, T. Kröll, N. Mărginean, T. Martinez, M.N. Mineva, C. Rossi-Alvarez, C.A. Ur, Unusual isospin-breaking and isospin-mixing effects in the $A = 35$ mirror nuclei, Phys. Rev. Lett. 92 (2004) 132502, http://dx.doi.org/10.1103/PhysRevLett.92.132502.

[21] D. Morrissey, B. Sherrill, M. Steiner, A. Stolz, I. Wiedenhoever, Commissioning the A1900 projectile fragment separator, Nucl. Insr. Meth. A 204 (2003) 90–96, http://dx.doi.org/10.1016/S0168-583X(02)01895-5, 14th International Conference on Electromagnetic Isotope Separators and Techniques Related to their Applications.

[22] O. Tarasov, D. Bazin, LISE++: Radioactive beam production with in-flight separators, Nucl. Instrum. Methods A 266 (19) (2008) 4657–4664, http://dx.doi.org/10.1016/j.nimb.2008.05.110, Proceedings of the XVth International Conference on Electromagnetic Isotope Separators and Techniques Related to their Applications.

[23] B. Longfellow, P. Bender, J. Belarge, A. Gade, D. Weisshaar, Commissioning of the LaBr3 (Ce) detector array at the national superconducting cyclotron laboratory, Nucl. Instrum. Methods Phys. Res. A 916 (2019) 141–147.

[24] W. Mueller, J. Church, T. Glasmacher, D. Gutknecht, G. Hackman, P. Hansen, Z. Hu, K. Miller, P. Quirin, Thirty-two-fold segmented germanium detectors to identify ˆi^3-rays from intermediate-energy exotic beams, Nucl. Instrum. Methods A 466 (3) (2001) 492–498, http://dx.doi.org/10.1016/S0168-9002(01)00257-1.

[25] C. Prokop, S. Liddick, B. Abromeit, A. Chemey, N. Larson, S. Suchyta, J. Tompkins, Digital data acquisition system implementation at the national superconducting cyclotron laboratory, Nucl. Instrum. Methods Phys. Res. A 741 (2014) 163–168.

[26] S. Agostinelli, et al., GEANT4 Collaboration, GEANT4: A simulation toolkit, Nucl. Instrum. Meth. A506 (2003) 250–303, http://dx.doi.org/10.1016/S0168-9002(03)01368-8.

[27] C. Ouellet, B. Singh, Nuclear data sheets for A=32, Nucl. Data Sheets 112 (9) (2011) 2199–2355.

[28] J. Chen, J. Cameron, B. Singh, Nuclear data sheets for A=35, Nucl. Data Sheets 112 (11) (2011) 2715–2850.

[29] E. Simpson, J.A. Tostevin, Two-nucleon correlation effects in knockout reactions from C 12, Phys. Rev. C 83 (1) (2011) 014605.